buildings

MDPI

Article

Seismic Behaviors of Double-Column Pier-Bearing System Based on Shaking Table Tests

Haiqing Zhu [1,*], Jianxin Li [1] and Yingqi Liu [2]

[1] School of Civil Engineering and Architecture, Wuhan Institute of Technology, Wuhan 430074, China; 22404010013@stu.wit.edu.cn
[2] School of Transportation and Logistics Engineering, Wuhan University of Technology, Wuhan 430063, China; selbyliu@whut.edu.cn
* Correspondence: hqzhu@wit.edu.cn

Abstract

In recent years, with the widespread application of double-column pier bridges, their seismic performance has attracted increasing attention. However, traditional seismic performance analysis treats piers and bearings as separate research objects, lacking an integrated investigation, which fails to provide accurate guidance for practical engineering projects. This paper aims to study the seismic performance of the double-column pier-bearing system based on shaking table tests. The results show that: (1) The sensitivity of the system's seismic performance indicators to bearings, ranked from highest to lowest, is: acceleration amplitude, damping ratio, displacement amplitude, and natural vibration frequency. (2) The cumulative effect of long-duration earthquakes is significant. Even with a lower peak ground acceleration, the displacement response may be greater than that of short-duration earthquakes with a higher peak ground acceleration. (3) Wavelet transform can accurately identify that the natural vibration frequency of systems equipped with different bearings ranges from 0.5 to 1.2 Hz, and the damping ratio ranges from 3% to 9%. (4) When the bearing thickness is increased from 21 mm to 42 mm, the system displacement response decreases from 11.41 mm to 10.28 mm. (5) Adding a 2 mm thick polytetrafluoroethylene layer to the conventional laminated rubber bearing can reduce the displacement response by 19%. The research findings indicate that it is necessary to conduct a feasibility analysis of bearing selection based on site characteristics.

Keywords: pier-bearing system; shaking table test; seismic performance; wavelet transform; bearing selection

Check for updates

Academic Editors: Weijing Zhang and Francisco López-Almansa

Received: 19 January 2026
Revised: 7 February 2026
Accepted: 13 February 2026
Published: 14 February 2026

Copyright: © 2026 by the authors. Licensee MDPI, Basel, Switzerland. This article is an open access article distributed under the terms and conditions of the Creative Commons Attribution (CC BY) license.

1. Introduction

In recent years, with the rapid advancement of transportation infrastructure construction, double-column pier bridges have been widely applied in highway and urban road network due to their advantages, such as simple structural form, high construction convenience, and good economic efficiency [1–5]. This type of bridge has become a core and important component of regional transportation systems, and its seismic safety and service reliability have attracted widespread attention.

Laminated rubber bearings are bridge bearings composed of alternating layers of rubber sheets and thin steel plates, bonded together via high-temperature vulcanization. As key force-transmitting components connecting the superstructure of bridges to the lower piers, their mechanical properties directly affect the dynamic response of the entire bridge

under earthquake action. To minimize the damage to bridge structures caused by strong earthquakes, laminated rubber bearings have become the most economical, practical, and easy-to-implement technical means in the field of bridge seismic isolation and vibration reduction [6,7]. Research findings based on bridge seismic damage investigations indicate that bearings play a significant role in reducing the probability of bridge seismic damage; if pre-deformed strains exist in the bearings, the probability of structural seismic damage increases significantly [8]. It had been confirmed that through experimental and numerical studies on the behavior of thick rubber bearings under tensile loads that these bearings can effectively reduce horizontal vibrations induced by earthquakes [9]. The multi-condition mechanical performance tests [10] on bearings through experiments combined with finite element analysis verified that the bearings can maintain stable stiffness even under 200% shear strain. Scaled model tests [11] to evaluate the seismic performance of bearings found that laminated rubber bearings can dissipate seismic energy through shear deformation and moderate sliding, thereby reducing the bending moment of bridge piers. The sliding phenomenon between bearings and beam bottoms [12] has been simulated and tested the effects of vertical compressive stress and sliding velocity on the friction coefficient. The results showed that the sliding of laminated rubber bearings can reduce the seismic force transmitted to the bridge piers. And a laminated rubber bearing with a sliding-shear cooperative layer obtained hysteretic curves within the shear strain range from 250% to 350% through quasi-static tests [13]. These tests verified that the energy dissipation and self-centering capabilities of the proposed bearing are superior to those of traditional laminated rubber bearings.

In addition, some scholars have verified the isolation performance of individual bearing parameters based on shaking table tests, such as laminated rubber bearings made of different materials, which were used to measure the sliding characteristics and energy dissipation capacity of the bearings under different embedding depths [14]. It was found that the sliding energy dissipation performance of natural rubber (NR) bearings is superior to that of chloroprene rubber (CR) bearings under long-period earthquakes. It has been investigated the influence of shape factors [15] on the buckling load of laminated rubber bearings, providing guidance for determining the thickness of rubber plates and the total rubber height in bearing design. Material properties of laminated rubber bearings have been studied using uniaxial tensile tests and finite element modeling [16], and the results showed that the horizontal stiffness of spiral laminated rubber bearings increased by 250% while the horizontal deformation decreased. Also, static and dynamic compression experiments on cylindrical chloroprene rubber specimens [17], providing experimental basis for clarifying the dynamic mechanical behavior of rubber bearings under pre-strain conditions.

Structural seismic response analysis involves analyzing the displacement, acceleration, internal force, or other responses of the entire system or local components to verify whether these indicators meet the requirements of corresponding codes, strength, stiffness, and other criteria, thereby avoiding severe damage or collapse during earthquakes [18,19]. However, in seismic response testing (such as shaking table tests and on-site measurements), raw signals inevitably contain noise, including zero drift of the sensor, ambient temperature changes, ground vibration, acquisition errors, and so on [20].

The wavelet transform method can be used to decompose raw signals into components of different frequency bands, which are then analyzed and processed to achieve denoising [21,22]. However, the effectiveness of wavelet transform is highly dependent on the selection of wavelet basis type, decomposition level, and threshold rule [23].

The above studies all indicate that laminated rubber bearings possess excellent seismic isolation performance and are a key technical means for the seismic reduction and

isolation design of bridges. However, previous studies have mostly focused on the local characteristics of piers or bearings, and systematic tests targeting the "double-column pier-bearing" system remain insufficient. This paper proposes to conduct shaking table tests on the double-column pier-bearing system. Starting from key indicators such as pier top displacement and acceleration amplification factor, Subsequently, wavelet transform is adopted to decompose and denoise the seismic displacement response signals, followed by the identification of natural vibration characteristics. Additionally, a sensitivity analysis of bearing parameters is conducted, aiming to clarify the influence law of key design parameters of bearings on the seismic performance of the double-column pier-bearing system and improving the efficiency of bridge bearing selection in seismic-prone areas.

2. Shaking Table Tests

2.1. Specimens and Installation

To reveal the isolation mechanism of the double-column pier-bearing system, the bridge model was designed with a 1:25 scale. The specific structural parameters are as follows: the pier column height is 1200 mm, and the cross-sectional diameter is 110 mm; the cap beam is a rectangular prism with dimensions of 700 mm (length) × 200 mm (width) × 100 mm (height), on which a 100 kg counterweight was placed to simulate the weight of the superstructure. The overall structural dimensions of the bridge are shown in Figure 1. C50 concrete is adopted for the main girders and bridge piers, in accordance with the specification "Code for design of concrete structures" [24], the standard value of cubic compressive strength of C50 concrete is 50 MPa, and the design value of axial compressive strength is 22.4 MPa. The longitudinal reinforcement consists of 4 steel bars with a diameter of 12 mm, adopting HRB335 (HRB stands for Hot-rolled Ribbed Bar), with a yield strength of 335 MPa. The stirrups have a diameter of 6 mm and a spacing of 200 mm, using HPB235 (HPB stands for Hot-rolled Plain Steel Bar), with a yield strength of 235 MPa. The specific reinforcement arrangement is shown in Figure 2.

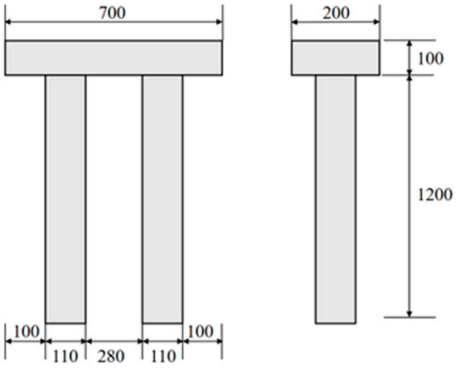

Figure 1. Bridge schematic diagram (unit: mm).

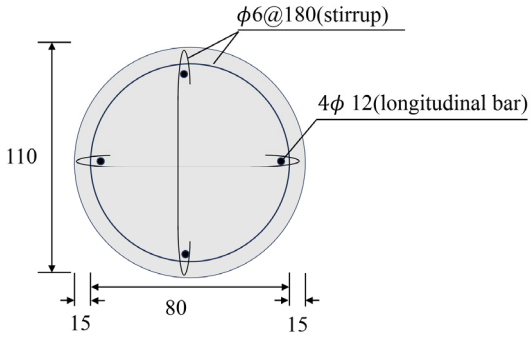

Figure 2. Pier reinforcement diagram (unit: mm).

To ensure the accurate transmission of shaking table excitation, the bottom of the pier was rigidly constrained using a fixed sleeve: the bottom of the pier was embedded into the sleeve, and through the tight fit between the sleeve and the pier body, as well as the preset positioning structure, the vertical displacement and horizontal movement of the pier during vibration were restricted, ensuring stable and reliable constraints, as shown in Figure 3.

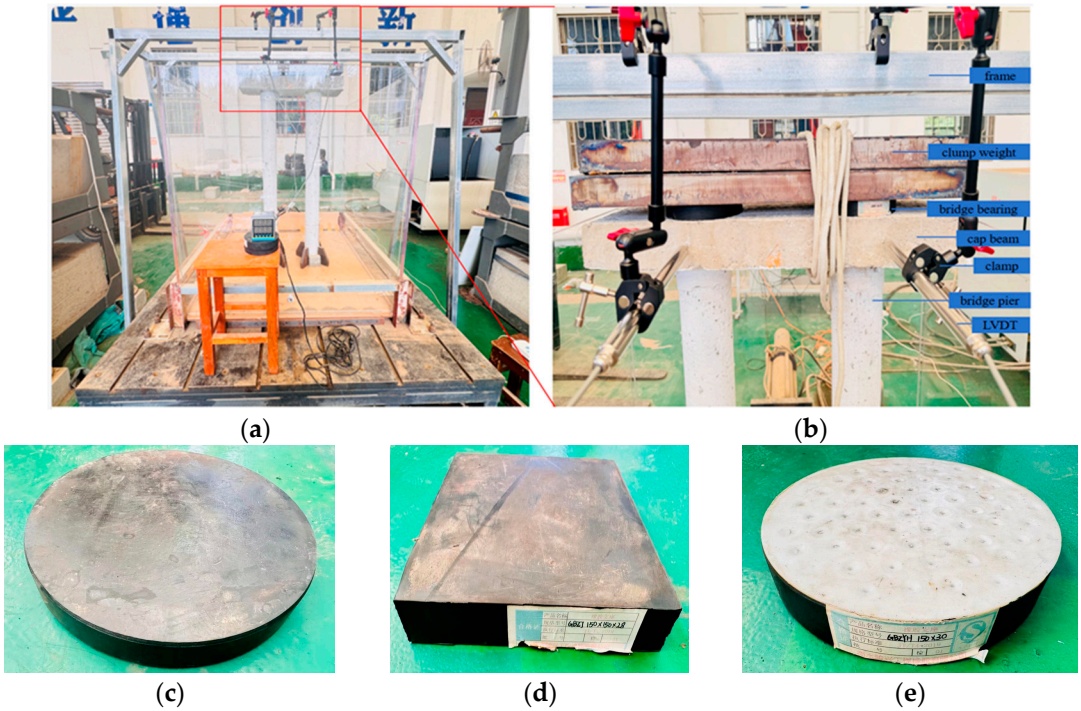

Figure 3. Loading set-up. (**a**) overall view; (**b**) enlarged view; (**c**) circular laminated rubber bearing; (**d**) square laminated rubber bearing; (**e**) PTFE–rubber bearing.

2.2. Testing Protocol and Measurement

With references [25–28], three typical ground motion records were selected as the shaking table input: Imperial Valley excitation (peak ground acceleration, PGA = 0.15 g) is a conventional ground motion, suitable for simulating the effects of moderate-to-low intensity stable seismic actions. Kobe excitation (PGA = 0.04 g) is a pulse-type near-fault ground motion, exhibiting significant destructive effects on long-period structures. And Taiwan Chi-Chi excitation (PGA = 0.06 g) is a hybrid-type ground motion, featuring both pulse characteristics and long duration, with obvious cumulative damage effects on structures. During the test, the acceleration time history of each ground motion was accurately input to the shaking table via a computer, driving the pier system to simulate earthquake action, and the seismic response data were obtained.

The test was conducted in the Structural Laboratory of Wuhan Institute of Technology. The test loading device was a unidirectional electro-hydraulic servo shaking table. The table plate is 1.8 m × 1.8 m, with a maximum load capacity of 10 t and an operating frequency range from 0.1 Hz to 50 Hz, which meets the test loading requirements. Displacement measurement was performed using a Linear variable differential transformer (LVDT) manufactured by Mirant (Atlanta, GA, USA), with a measuring range of 50 mm, a measurement accuracy of 5 μm. One end of the sensor was closely attached to the cap beam, and the other end was fixed to the reaction frame via a metal fixture. To prevent the sensor from sliding relative to the reaction frame, a rubber anti-slip pad was placed between the fixture and the reaction frame, shown in Figure 3b. The bearings are shown as Figure 3c–e.

According to practical experience [29,30], 7 test conditions were designed, focusing on the quantitative effects of four parameters, including bearing thickness, shape, type, and material. The pier top displacement, acceleration amplification factor, free vibration frequency and damping ratio were studied. The parameter combinations of each working condition are detailed in Table 1. The bearing thicknesses are 21, 28, 35, and 42 mm, respectively; the shapes are circular and square; the types involve laminated bearings and polytetrafluoroethylene (PTFE)-rubber bearings; and the materials are chloroprene rubber (CR) and natural rubber (NR).

Table 1. Test conditions and parameter combinations.

No.	Thickness (mm)	Material	Shape	Type
1	21	CR	Circular	Laminated rubber bearing
2	28	CR	Square	Laminated rubber bearing
3	28	CR	Circular	Laminated rubber bearing
4	30 *	CR	Circular	PTFE–rubber bearing
5	35	NR	Circular	Laminated rubber bearing
6	35	CR	Circular	Laminated rubber bearing
7	42	CR	Circular	Laminated rubber bearing

* 30 mm bearing consists of 28 mm laminated rubber and 2 mm polytetrafluoroethylene sheet.

2.3. Indicators for Seisminc Performance

Some scholars have conducted research on the seismic performance of laminated rubber bearing beam bridges [31,32]. In these research, four indicators—peak pier top displacement (Δ_p), acceleration amplification factor (*AMF*), natural frequency (f), and damping ratio (ξ)—were selected for analysis in this study. The definition and calculation method of each indicator are as follows: Δ_p refers to the maximum horizontal displacement generated at the pier top under earthquake action. As the most intuitive indicator reflecting the structural displacement response, its magnitude holds irreplaceable academic and engineering value in the seismic safety evaluation of bridges and post-earthquake emergency decision.

The *AMF* refers to the ratio of the peak horizontal acceleration at the pier top to the peak input acceleration of the shaking table. It reflects the amplification or attenuation effect of the system on ground motion. If $AMF > 1$, it indicates that the target location has an "amplification effect" on acceleration, if $AMF < 1$, it indicates an "attenuation effect", and if $AMF = 1$, it indicates no amplification or attenuation. From the perspective of past earthquake damage patterns [33,34], transverse damage to bridges is rare, while longitudinal damage to piers and bearings caused by excessive longitudinal displacement is more common. Therefore, this study focuses on the longitudinal displacement of piers for analysis.

With references [35–37], it is found that the acceleration amplification factor can be calculated using the following formula:

$$AMF = \frac{A_{top}}{A_{base}} \tag{1}$$

where A_{top} is the peak acceleration at the pier top whose value is obtained by performing the second-order differential operation on the pier top displacement time-history data collected in the test; A_{base} is the peak input acceleration of the shaking table.

The natural frequency can be calculated using Equation (2):

$$f = \frac{1}{T} \tag{2}$$

where T is the vibration period and can be obtained from measured vibration data.

The damping ratio can be calculated using Equation (3):

$$\xi = \frac{1}{2\pi n} \ln \frac{y_k}{y_{k+n}} \tag{3}$$

where n is the number of vibrations during the observation phase, y_k represents the amplitude at the start of the observation phase (i.e., the amplitude of the k-th cycle), and y_{k+n} represents the amplitude at the end of the observation phase (i.e., the amplitude of the (k+n)-th cycle).

3. Seismic Performance Analysis

3.1. Influence of Bearing Thickness

3.1.1. Intuitive Analysis

To investigate the influence of the thickness of laminated rubber bearings on the seismic performance of bridges, loading conditions 1, 3, 6, and 7 were grouped for analysis, with the bearing thicknesses being 21, 28, 35, and 42 mm, respectively. The test results show that the seismic performance of the system improves with the increase in bearing thickness. The displacement time responses are shown in Figure 4 and the specific seismic performance indicators are presented in Table 2.

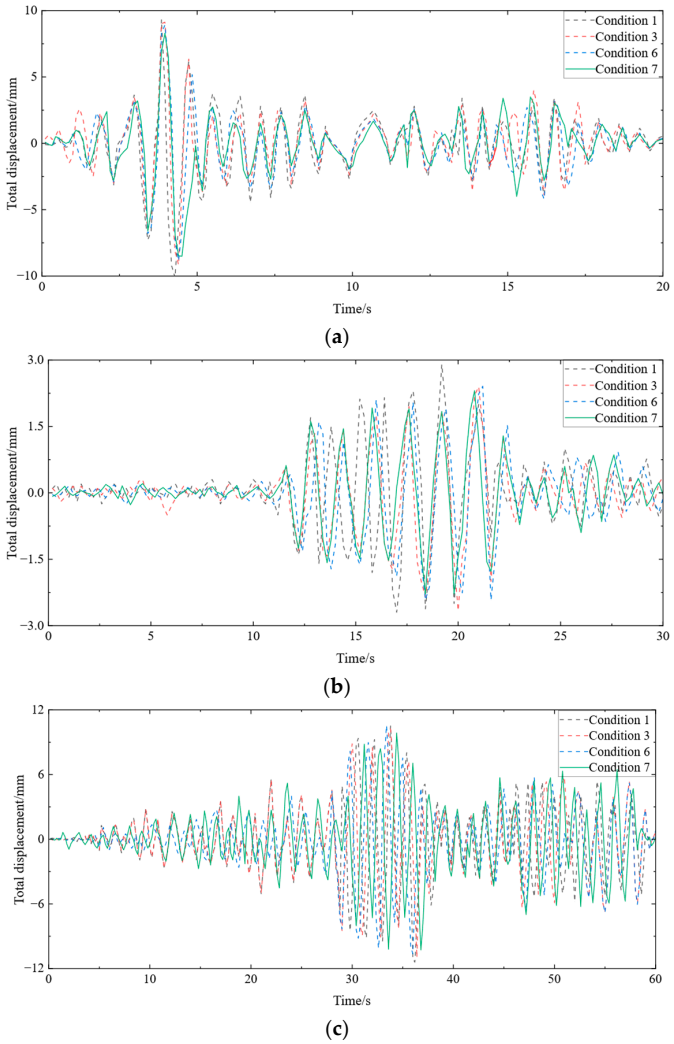

Figure 4. Pier top displacement history curves. (**a**) Imperial Valley; (**b**) Kobe; (**c**) Chi-Chi.

Table 2. The influence of bearing thickness on seismic indicators.

No.	t (mm)	Imperial Valley				Kobe				Chi-Chi			
		Δ_p (mm)	*AMF*	f	ξ	Δ_p (mm)	*AMF*	f	ξ	Δ_p (mm)	*AMF*	f	ξ
1	21	10.12	0.697	0.799	8.9%	2.90	0.225	0.536	7.9%	11.41	0.588	0.410	9.7%
3	28	9.14	0.472	0.992	5.9%	2.66	0.202	0.592	6.2%	10.96	0.441	0.574	6.9%
6	35	8.91	0.464	0.992	4.5%	2.42	0.174	0.592	4.9%	10.64	0.350	0.574	6.0%
7	42	8.51	0.416	0.992	3.8%	2.31	0.161	0.592	5.8%	10.28	0.320	0.656	4.1%

From the perspective of pier displacement response, the effects of seismic excitations on the system in descending order are Chi-Chi, Imperial Valley, and Kobe, with the pier top displacements being approximately 10.8 mm, 8.9 mm, and 2.6 mm, respectively. In addition, under various seismic excitations, an increase in bearing thickness leads to a slight reduction in peak displacement. For example, under the Imperial Valley excitation, when the bearing thickness is doubled from 21 mm to 42 mm, the value of Δ_p is decreased from 10.12 mm to 8.51 mm, only reduced by about 10% (i.e., the ratio of the difference between the maximum and minimum values to the maximum value). Generally, as the bearing thickness increases, both the maximum allowable lateral and vertical deformation capacities of the bearing increase. The bearing absorbs more energy through its own deformation, thereby reducing the transmission of seismic energy to the superstructure.

The instantaneous acceleration responses are presented in Figure 5. It can be seen that although the bearing thickness increases, the trends of the acceleration responses remain quite similar. However, the maximum *AMF* value is larger for the loading conditions with smaller bearing thicknesses. For instance, under the Imperial Valley excitation, the maximum *AMF* value decreases by approximately 68% when the bearing thickness is increased from 21 mm to 42 mm.

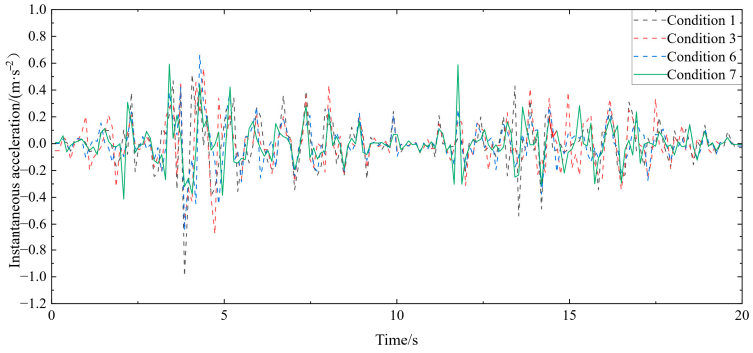

(**a**)

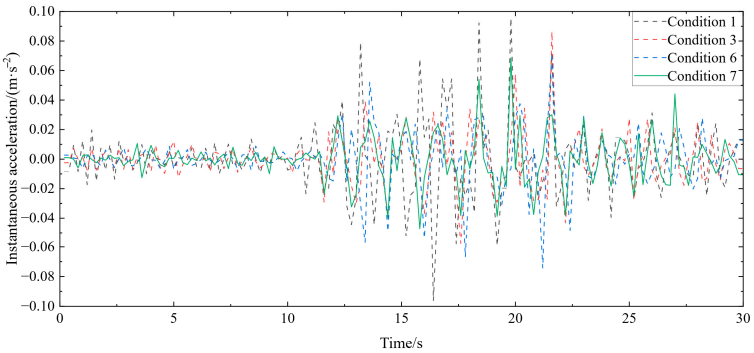

(**b**)

Figure 5. *Cont.*

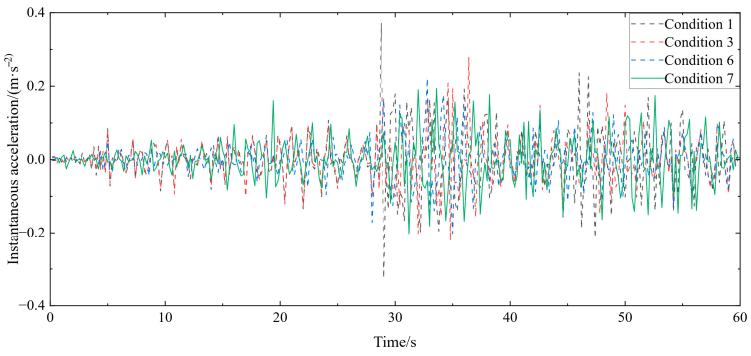

(**c**)

Figure 5. *AMF* response curves. (**a**) Imperial Valley; (**b**) Kobe; (**c**) Chi-Chi.

Both of the above phenomena indicate that increasing the bearing thickness has a certain positive effect on improving the seismic performance of the system. However, the differences among the displacement time histories are too small. Therefore, the wavelet transform method is introduced to decompose the displacement response components, so as to conduct a more detailed study on the free vibration characteristics of the pier system.

3.1.2. Free Vibration Analysis

The time-history signals of seismic displacement response of piers are mostly complex signals with non-stationary and multi-frequency components. Traditional Fourier transform is difficult to accurately capture the variation law of their frequency components over time. Based on the principle of multi-resolution analysis, wavelet transform can conduct multi-scale refinement of signals through scaling and translation operations. It can not only analyze the overall frequency distribution of signals, but also focus on local time-domain characteristics, which is fully suitable for the analysis requirements of pier seismic response signals [38–41]. In the field of structural dynamics, wavelet transform has been successfully applied to scenarios such as vibration signal denoising and modal parameter identification, providing a mature theoretical and practical basis for its application in pier seismic response analysis.

In this paper, in order to extract the free vibration characteristics, a MATLAB program for decomposing time-history signal components was compiled. The sampling intervals of the Imperial Valley, Kobe and Chi-Chi excitations are 0.11 s, 0.2 s, and 0.2 s, respectively. The sampling frequency is automatically identified in the wavelet transform program, which is equal to the reciprocal of the acceleration time interval. In the program, the wavelet basis function is manually input, with optional types including dbN, coifN, symN, and so on. The number of wavelet decomposition layers is set to 3. The start and end times for the calculation of the natural vibration frequency are manually input, as are the lower and upper limits of the natural vibration frequency.

Firstly, the displacement components were decomposed into ultra-low frequency components, low frequency components, medium frequency components and high frequency components, which respectively refer to the structural baseline drift components, pier free vibration components, seismic excitation components, as well as high-order vibration and noise components. Taking loading condition 1 under the action of Imperial Valley wave as an example, the sym8 wavelet basis was selected, and according to the frequency characteristics of seismic excitation, the original time-history signal was decomposed into ultra-low frequency components (<0.5 Hz), low frequency components (0.5~1.2 Hz), medium frequency components (1.5~2.5 Hz) and high frequency components (>2.5 Hz), as shown in Figure 6. It should be noted that trial calculations revealed that different wavelet bases need to be selected for displacement time histories induced by different seismic

excitations. Common wavelet bases provided by MATLAB 2025a software include db4, db6, sym8, coif4, etc. The criterion for selecting the most suitable wavelet basis is that the separated free vibration component time history should exhibit an approximately sine or cosine waveform.

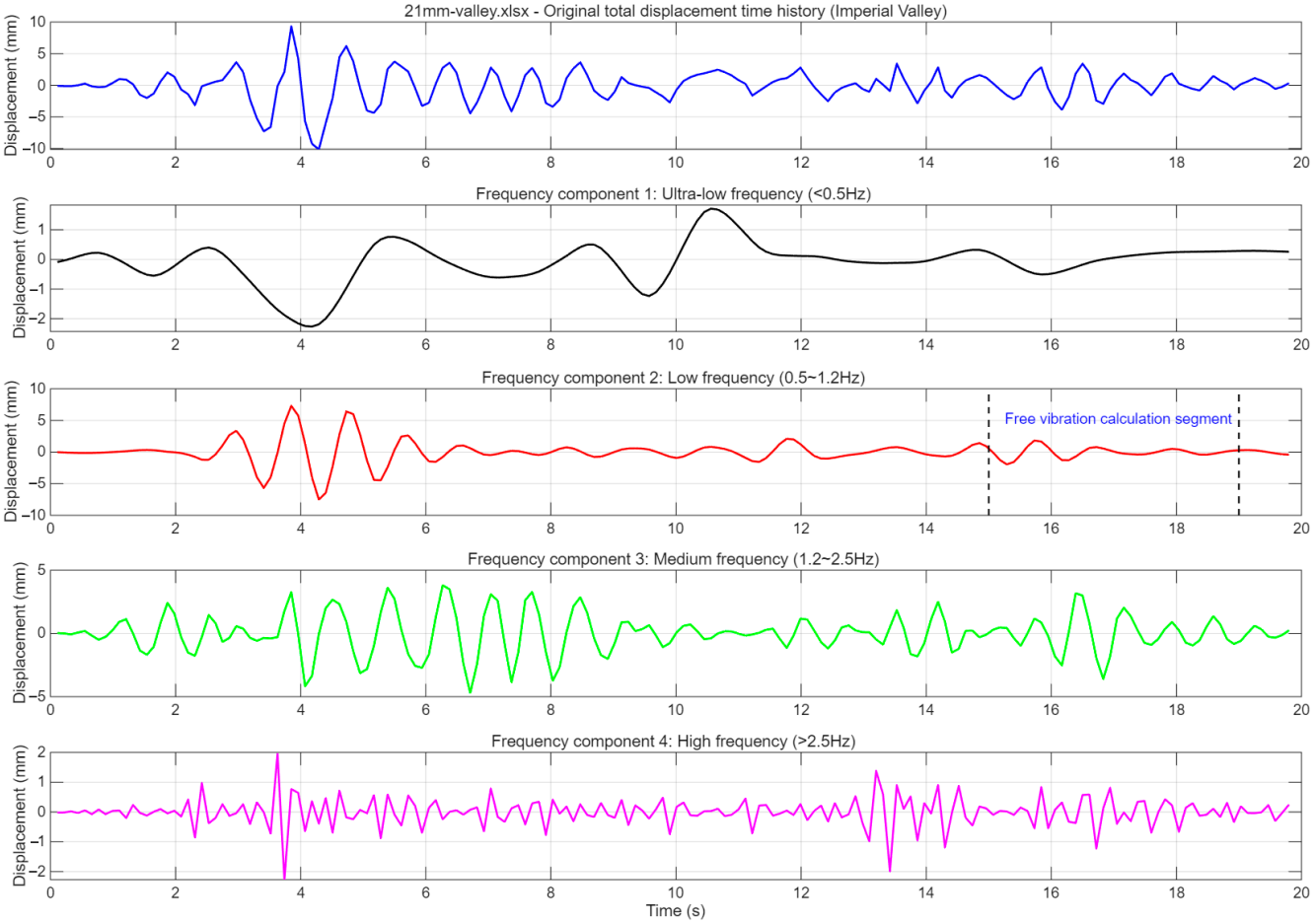

Figure 6. Displacement component decomposition diagram (21 mm, Imperial Valley).

Then, the free vibration characteristics were extracted. For the free vibration components (i.e., low frequency component signals), a segment of signal closest to cosine was selected, and the free vibration frequency and damping ratio were calculated using Equation (2) and Equation (3), respectively. For example, the 4~8 s or 15~19 s of the red signal line in Figure 6 was selected as the analysis segment for free vibration characteristics. In fact, the calculation results of these two segments were almost the same. Trial calculations showed that the latter segment of other conditions was more likely to approximate the free vibration waveform. Therefore, in batch parameter analysis, the latter segment was selected as the free vibration characteristic extraction segment. Due to space limitations, only the analysis process of this condition is presented, and the calculation results of all analyses are shown in Table 2.

Overall, wavelet transform can accurately identify the free vibration frequency of the system. In Table 2, the calculated values of free vibration frequency are in the range of 0.5~1.2 Hz; moreover, under the same excitation, increasing only the bearing thickness results in almost no change in free vibration frequency. This phenomenon is consistent with the actual situation, i.e., the influence of damping on free vibration frequency is negligible.

Furthermore, wavelet transform can reasonably identify the damping ratio of the system. On the whole, the damping ratio values of all loading conditions are in the range

of 3~9%, which is a reasonable damping ratio for reinforced concrete structures. From each row of Table 2, for example, the damping ratios of the case with a thickness of 21 mm under different excitations are 8.9%, 7.9%, and 8.2%, respectively, which are relatively close to each other. The calculated damping ratio values of other working conditions also exhibit the same phenomenon.

However, looking through each column of Table 2, the peak displacement decreases with the increase in bearing thickness, and the damping ratio also decreases with the increase in bearing thickness, i.e., smaller peak displacement values and smaller damping ratio values appear in pairs. Nevertheless, according to the results solved by the dynamic equation, larger peak displacement values should be accompanied by smaller damping ratio values. But the measured variation trend is opposite to that of the theoretical solution. The core reason is that the test system is a rubber bearing–pier coupling system, where the bearing not only functions to provide damping but also exerts an influence on the system stiffness. In fact, the seismic response of this system is dominated by stiffness: increasing the bearing thickness raises the system stiffness, thereby reducing the system's displacement response; meanwhile, increasing the bearing thickness also decreases the system damping, which in turn increases the system's displacement response. However, the magnitude of the displacement reduction induced by the former is far greater than that of the displacement increase caused by the latter, which thus leads to the measured pattern that the peak displacement and damping ratio decrease synchronously.

3.2. Influence of Bearing Shape

A comparative study was conducted on the influence of bearing shapes on the system's seismic responses under different seismic excitations. All bearings had a thickness of 28 mm, where condition 2 adopted square bearing and condition 3 adopted circular bearing. The collected Δ_p values were listed in Table 3; meanwhile, the total displacement responses, natural vibration component responses and seismic component responses derived from wavelet transform were plotted in Figure 7, with the corresponding natural vibration characteristic index values presented in Table 3.

Table 3. The influence of bearing shape on seismic index.

No.	Shape	Imperial Valley				Kobe				Chi-Chi			
		Δ_p (mm)	*AMF*	*F*	ξ	Δ_p (mm)	*AMF*	*f*	ξ	Δ_p (mm)	*AMF*	*f*	ξ
2	Square	9.88	0.551	0.992	3.4%	2.86	0.220	0.588	2.6%	11.58	0.661	0.588	3.6%
3	Circular	9.14	0.472	0.992	5.9%	2.66	0.202	0.592	6.2%	10.96	0.441	0.574	6.9%

From the perspective of total displacement responses, the qualitative conclusion is that the vibration reduction effect of circular bearings is slightly better than that of square bearings. Under these three excitations, the Δ_p of the system with circular bearings is 7%, 7%, and 5% lower than that of the system with square bearings, respectively. This is because, under any seismic excitation, the peak displacement of the system with circular bearings is smaller than that with square bearings. Additionally, the *AMF* of circular bearings is smaller than those of square bearings, and the damping ratio of circular bearings are higher than those of square bearings.

Further investigation on the natural vibration component responses reveals that under Imperial Valley excitation, the vibration periods and peak occurrence times of the two cases are almost identical, but the peak value of condition 2 is 3 mm smaller than that of condition 3. Under Kobe excitation and Chi-Chi excitation, the vibration periods of the natural vibration component responses for the two cases are nearly the same; the peak of

condition 2 appears slightly earlier than that of condition 3, and the absolute values of the peaks of the two cases are almost equal. Furthermore, under the three types of excitations, the damping ratio of the system with circular bearings is 42%, 58%, and 48% higher than that of the system with square bearings, respectively.

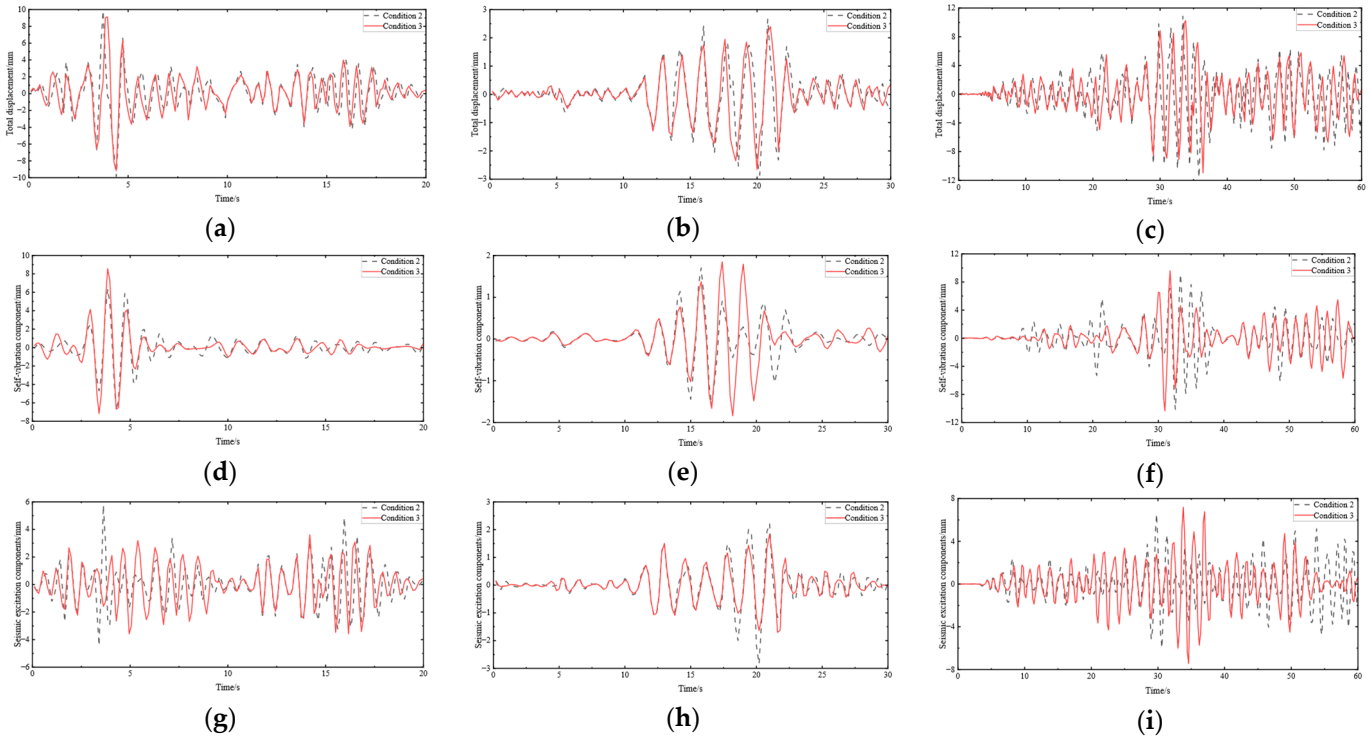

Figure 7. Pier top displacement time-history curves. (**a**) Imperial Valley, total displacement response; (**b**) Kobe, total displacement response; (**c**) Chi-Chi, total displacement response; (**d**) Imperial Valley, free vibration component; (**e**) Kobe, free vibration component; (**f**) Chi-Chi, free vibration component; (**g**) Imperial Valley, seismic excitation component; (**h**) Kobe, seismic excitation component; (**i**) Chi-Chi, seismic excitation component.

These findings indicate that circular bearings exhibit superior seismic performance compared to square bearings.

3.3. Influence of Bearing Type

Using polytetrafluoroethylene (PTFE) layers is a common measure to reduce friction between solid surfaces. Therefore, it also has broad application prospects in bridge bearings. The PTFE–rubber bearing is a type of bearing that integrates load-bearing, seismic isolation and sliding functions.

Laminated rubber bearings are formed by alternating lamination and vulcanization of multiple layers of neoprene sheets and thin steel plates. They rely on rubber shear deformation to provide horizontal displacement and rotational capacity, featuring high vertical stiffness, simple structure, low cost, and a working temperature ranging from −25 °C to 30 °C. They are suitable for medium and small-span bridges with spans $\leq$ 30 m and small displacements.

PTFE–rubber bearings are based on laminated rubber bearings, with a polytetrafluoroethylene sheet bonded to the top surface, forming a low-friction sliding pair ($\mu \leq 0.03$) with the stainless steel plate at the beam bottom. Their horizontal displacement is not limited by rubber shear, making them suitable for long-span bridges and movable ends with large displacements. Their vertical performance is consistent with that of laminated rubber bearings, while their cost is 30% higher.

In this study, condition 3 and 4 correspond to the rubber bearing and PTFE–rubber bearing, respectively. The only difference is that the latter has an additional 2 mm thick PTFE layer compared to the former. The peak displacements observed in the shaking table tests were listed in Table 4, while the original displacement responses and displacement component responses were presented in Figure 8.

Table 4. The influence of bearing type on seismic indicators.

No.	Type	Imperial Valley				Kobe				Chi-Chi			
		Δ_p (mm)	*AMF*	f	ξ	Δ_p (mm)	*AMF*	f	ξ	Δ_p (mm)	*AMF*	f	ξ
3	Laminated rubber bearing	9.14	0.472	0.992	5.9%	2.66	0.202	0.592	6.2%	10.96	0.441	0.574	6.9%
4	PTFE–rubber bearing	8.47	0.427	0.727	6.1%	2.26	0.169	0.392	8.5%	8.89	0.328	0.574	6.8%

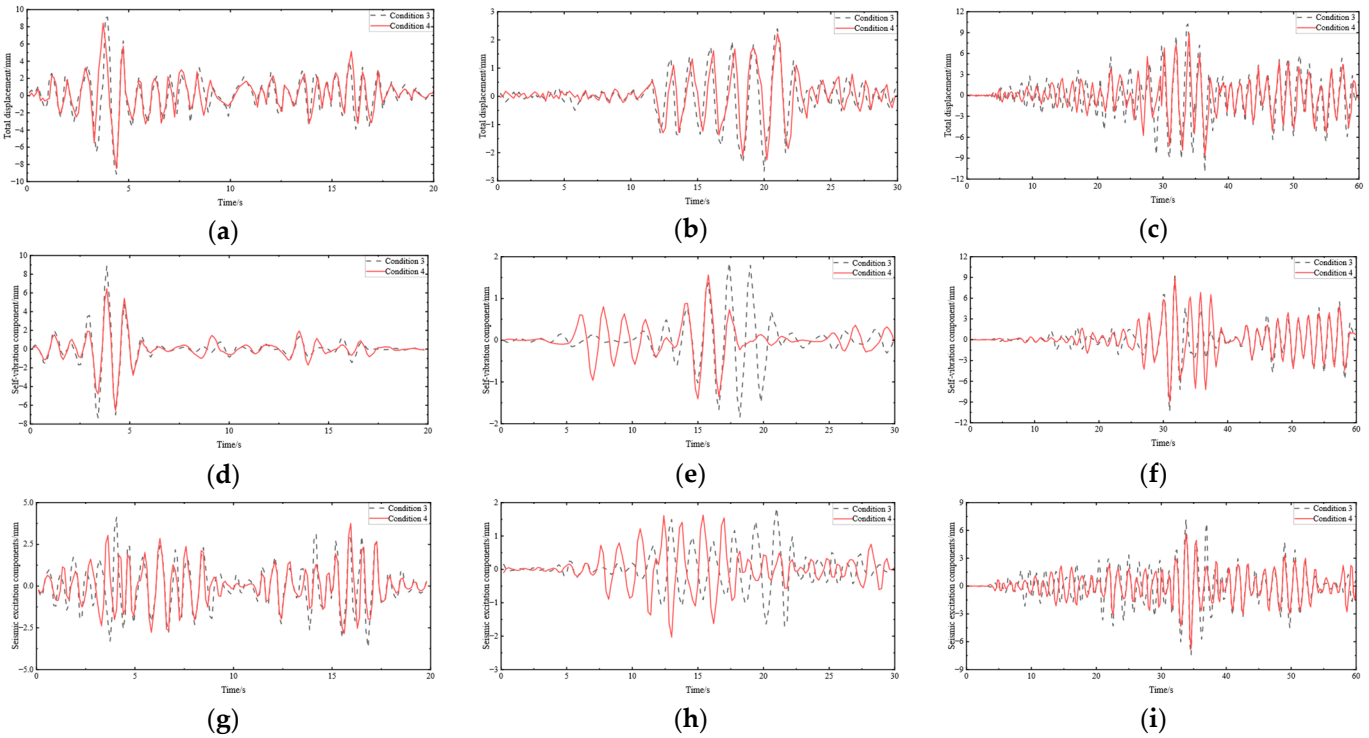

Figure 8. Pier top displacement time-history curves. (**a**) Imperial Valley, total displacement response; (**b**) Kobe, total displacement response; (**c**) Chi-Chi, total displacement response; (**d**) Imperial Valley, free vibration component; (**e**) Kobe, free vibration component; (**f**) Chi-Chi, free vibration component; (**g**) Imperial Valley, seismic excitation component; (**h**) Kobe, seismic excitation component; (**i**) Chi-Chi, seismic excitation component.

Overall, using PTFE material provides a vibration reduction effect, as both the peak displacement and *AMF* of condition 3 are larger than those of condition 4. The outline of the black dashed line in Figure 8 is larger than that of the red solid line, indicating that both the free vibration component response and the seismic excitation component response of condition 3 are greater than those of condition 4.

In detail, adding a single 2 mm thick PTFE layer can reduce the peak displacements under the three excitation cases by 7%, 15%, and 19% in sequence, leading to a slight decrease in the natural vibration frequency, while the damping ratio shows no significant change. The results indicate that the PTFE layer, as a key component of seismic isolation bearings,

does not directly provide damping or stiffness. Instead, it leverages its material properties of low friction and self-lubrication to allow relative displacement between the bearing and the superstructure. The static friction coefficient between the PTFE layer and the stainless steel plate is less than 0.05 at room temperature, meaning that slight perturbations under seismic excitation can induce horizontal displacement of the bearing, thus preventing excessive horizontal forces from being transmitted to the superstructure. This indicates that the PTFE material exerts a distinct seismic isolation effect on the superstructure.

However, from the second and third rows of images in Figure 8, the wavelet transform analysis of the responses under the Imperial Valley excitation and Chi-Chi excitation is more stable; for the Kobe excitation (i.e., the excitation with lower energy), the analysis accuracy is unstable. Because a phase difference occurs between the black and red waves in both Figure 8e,h. The PGA of the Kobe excitation is set to 0.04 g; consequently, the total energy of the response induced thereby is relatively low, and the energy of each component of the response is low with no significant differences to each other. The principle of wavelet transform lies in extracting signal components through the resonance between wavelet basis functions and the original signal. Furthermore, the Kobe excitation is a pulse-type excitation, and the number of waves available for extracting the natural vibration characteristics is small, leading to a relatively large error. For these reasons, the wavelet transform exhibits unstable performance when applied to analyze the response induced by the Kobe excitation.

3.4. Influence of Bearing Material

To investigate the influence of the material of laminated rubber bearings on the seismic performance of bridges, Working Conditions 5 and 6 were grouped for analysis. The two bearing materials used in this test were chloroprene rubber and natural rubber, the thickness of the bearings are the same.

Natural rubber (NR) is a type of natural polymer material, produced by processing the latex secreted by rubber trees through such procedures as coagulation and drying. It boasts excellent elasticity and a fast rebound rate. The elastic modulus of natural rubber at room temperature is approximately 0.3~0.6 MPa. However, it has poor aging resistance and tends to crack when exposed to oxygen, ozone, and ultraviolet radiation, thus requiring the addition of anti-aging agents.

Chloroprene rubber (CR) [42] is a synthetic polymer material, formed by the polymerization of chloroprene monomers. Its rebound performance is inferior to that of natural rubber. The elastic modulus of natural rubber at room temperature is approximately 0.8~1.5 MPa. With outstanding aging resistance, it also exhibits excellent ozone and weather resistance and is not prone to cracking, hence earning the reputation of the "universal rubber".

The results directly measured in the tests are listed in Table 5, and the outcomes of wavelet transform are presented in Table 5 and Figure 9. Under all excitations, both the Δ_p and the *AMF* of condition 5 are smaller than those of condition 6, while the natural vibration frequency of condition 5 is approximately equal to that of condition 6. Under long-duration seismic excitations, the damping ratio of condition 5 is higher than that of condition 6. Preliminarily, the seismic performance of the system equipped with NR bearings outperforms that of the system with CR bearings.

Table 5. The influence of bearing material on seismic indicators.

No.	Material	Imperial Valley				Kobe				Chi-Chi			
		Δ_p (mm)	*AMF*	f	ξ	Δ_p (mm)	*AMF*	f	ξ	Δ_p (mm)	*AMF*	f	ξ
5	NR	8.28	0.330	0.799	9.4%	2.18	0.136	0.588	3.9%	10.38	0.331	0.556	9.5%
6	CR	8.91	0.464	0.992	4.5%	2.42	0.174	0.592	4.9%	10.64	0.350	0.574	6.0%

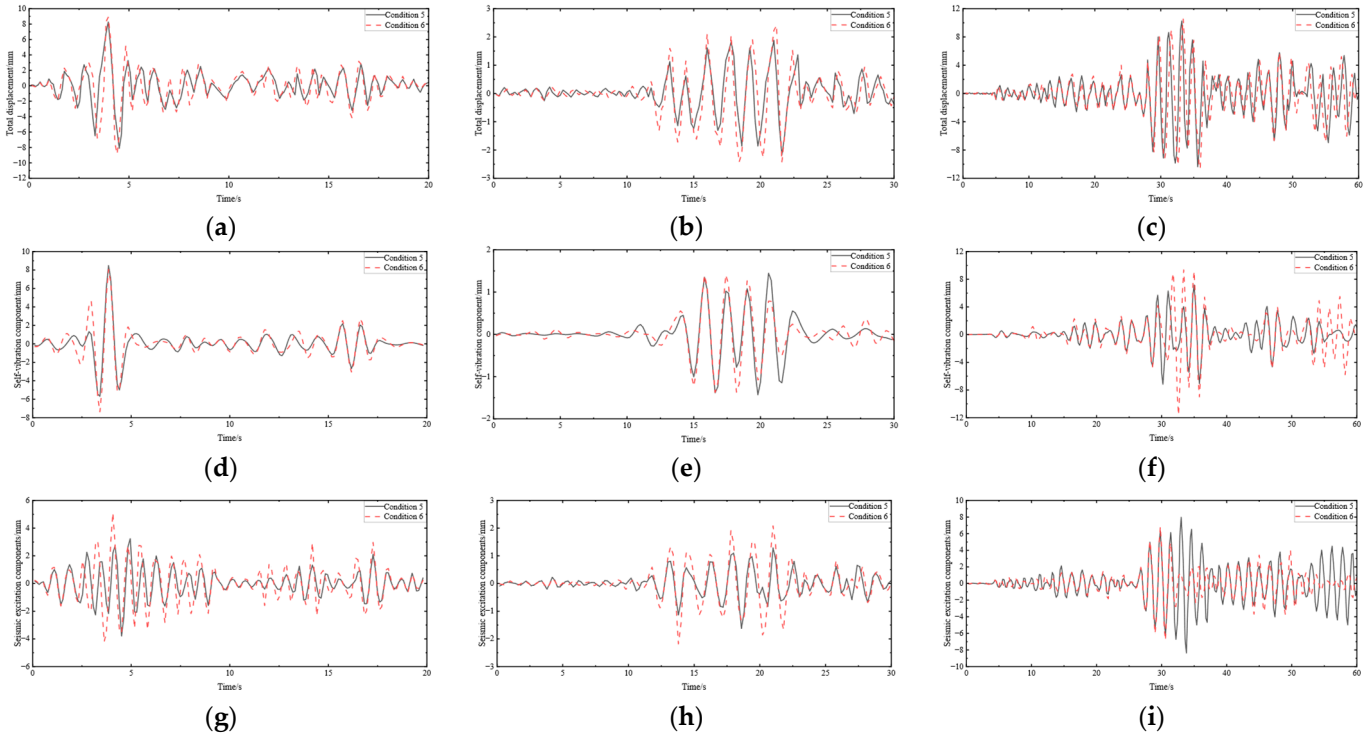

Figure 9. Pier top displacement time-history curves. (**a**) Imperial Valley, total displacement response; (**b**) Kobe, total displacement response; (**c**) Chi-Chi, total displacement response; (**d**) Imperial Valley, free vibration component; (**e**) Kobe, free vibration component; (**f**) Chi-Chi, free vibration component; (**g**) Imperial Valley, seismic excitation component; (**h**) Kobe, seismic excitation component; (**i**) Chi-Chi, seismic excitation component.

The reason why both the Δ_p and the *AMF* of condition 5 are lower than those of condition 6 is mainly that the elastic modulus of NR is smaller than that of CR. Specifically, a lower elastic modulus corresponds to greater deformation capacity; the bearings dissipate energy through their own deformation, thereby reducing the displacement of the structural system.

From the perspective of the natural vibration component responses in the second row of Figure 9, under various excitations, the vibration of condition 5 returns to the vicinity of the equilibrium position more rapidly than that of condition 6, indicating that the damping ratio of condition 5 is higher than that of condition 6. A higher damping ratio results in a smaller response peak under external loads; thus, in the seismic component responses shown in the third row of Figure 9, the peaks of condition 5 are smaller than those of condition 6.

Regardless of the type of excitation or the type of wavelet, the identified natural vibration frequency of the pier system in this study ranges from 0.5 to 1.2 Hz. Essentially, this system exhibits the most significant response to excitations in the low-frequency range and is thus more prone to resonance. NR features a low elastic modulus and low stiffness, leading to a low vibration frequency and a long vibration period. In contrast, CR has

a high elastic modulus and high stiffness, resulting in a high vibration frequency and a short vibration period. Therefore, NR bearings should be selected when it is necessary to extend the structural period to avoid resonance; CR bearings are preferred when increased structural stiffness is required to reduce displacement responses.

In addition, wavelet transform exhibits a certain limitation in separating the responses of pulse-type signals. It is necessary to select a series of consecutive peaks with gradually decreasing values and calculate the damping ratio using Equation (3). However, the number of available peaks for the pulse-type response in Figure 9e is insufficient, which may lead to deviations in the calculation results. This also accounts for the phenomenon that the damping ratio of natural rubber bearings is found to be higher than that of chloroprene rubber bearings under the Imperial Valley and Chi-Chi excitations, whereas the opposite trend is observed under the Kobe excitation.

4. Analysis of Pier Stability

A core evaluation criterion for pier stability is the allowable displacement of piers defined in the specification (JTG/T 2231-01-2020, Code for Seismic Design of Highway Bridges), which refers to the maximum horizontal displacement limit that a pier can sustain to maintain its load-bearing capacity and avoid irreparable damage or collapse under earthquake action. The calculation needs to incorporate parameters such as pier height, section equivalent yield curvature, maximum allowable rotation angle of plastic hinges, and equivalent plastic hinge length.

The formula for calculating the allowable displacement of the single-column pier is as follows:

$$\Delta u = \frac{1}{3}H^2 \cdot \varphi_y + \left(H - \frac{L_p}{2}\right) \cdot \theta_u \tag{4}$$

$$L_{p1} = 0.08H + 0.022 f_y d_s \geq 0.044 f_y d_s \tag{5}$$

$$L_{p2} = \frac{2}{3}b \tag{6}$$

$$L_p = \min\left(L_{p1}; L_{p2}\right) \tag{7}$$

where H is the height of the cantilever pier (cm). φ_y is the equivalent yield curvature of the section (1/cm). θ_u is the maximum allowable rotation angle of the plastic hinge region. L_p is the equivalent plastic hinge length (cm), which is the smaller value of the calculation results of Equations (4) and (5). b is the diameter (cm) of the circular cross section. f_y is the standard value of tensile strength of longitudinal steel bar (MPa). d_s is the diameter (cm) of the longitudinal reinforcement.

The allowable displacement calculated using the single-column pier allowable displacement method recommended in the specification is 52.5 mm. The allowable displacement of the double-column pier system in this study should be greater than 52.5 mm.

Generally, the Imperial Valley excitation (0.15 g) is representative of moderate-intensity, short-duration, high-frequency non-pulse-type ground motion, which is used to verify the energy dissipation capacity of short-period structures under conventional earthquakes. The Kobe excitation (0.04 g) represents low-intensity, extremely short-duration, high-frequency pulse-type ground motion, which is adopted to evaluate the instantaneous seismic resistance of short-period components. The Chi-Chi excitation (0.06 g) is typical of low-intensity, long-duration, broadband ground motion, which is applied to investigate the cumulative damage of structures under long-duration seismic excitation.

Figure 10 presents the results of pier stability analysis. The peak displacement is represented by columns, with specific values read from the left vertical axis; the *AMF* is depicted by lines, with corresponding values checked against the right vertical axis. In

this study, the PGAs of the Imperial Valley, Kobe and Chi-Chi earthquake excitations were set to 0.15 g, 0.04 g and 0.06 g, respectively. The corresponding peak displacements of the system under these excitations are approximately 9.0 mm, 2.5 mm and 10.6 mm, which are much lower than the code-specified allowable value of 52.5 mm. Although the PGA of the Chi-Chi excitation is significantly lower than that of the Imperial Valley excitation, the corresponding displacement response is relatively larger, indicating that the cumulative effect of long-duration excitation cannot be ignored.

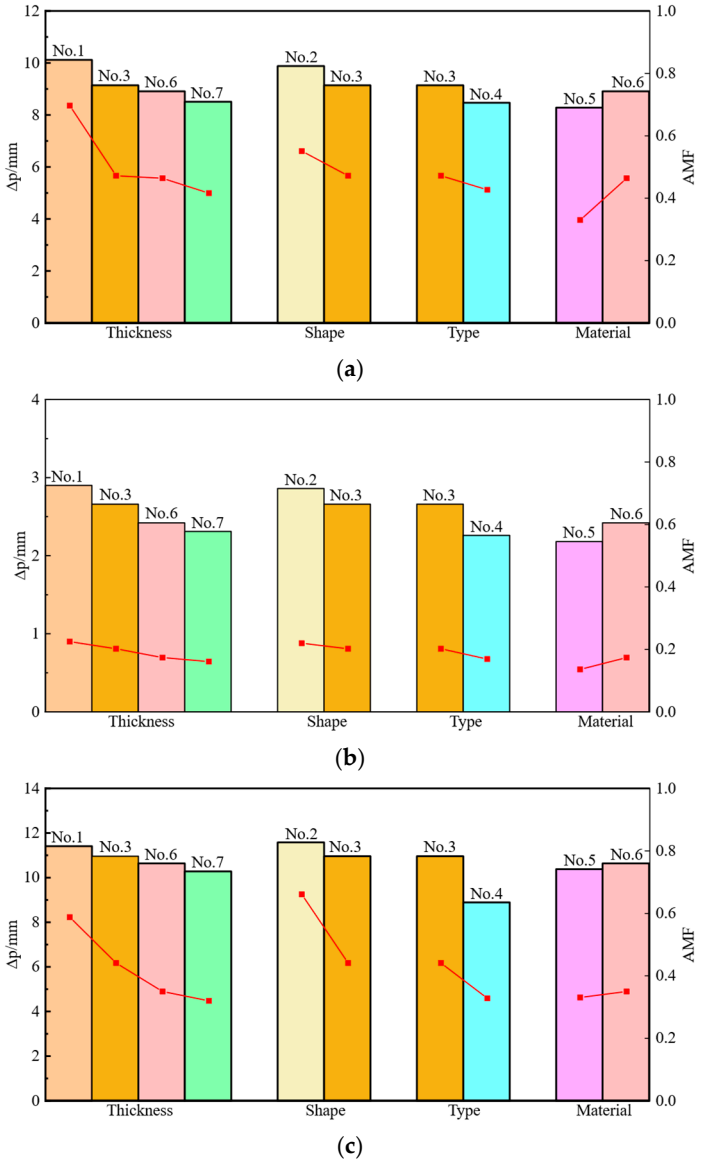

Figure 10. Displacement overrun analysis. (**a**) Imperial Valley; (**b**) Kobe; (**c**) Chi-Chi.

Moreover, the average *AMF* values under the three excitations are 0.48, 0.18, and 0.43, respectively., all of which are less than 1, demonstrating that the inherent damping of the system can mitigate the effect of seismic excitation on the superstructure. However, the PGA of the Chi-Chi excitation is much smaller than that of the Valley excitation; thus, this phenomenon indicates that the acceleration response is more sensitive to long-duration excitations. In detail: as the bearing thickness increases from 21 mm to 42 mm, the *AMF* values decrease by 40%, 28% and 52%, respectively. Furthermore, the *AMF* values of the square bearing system are higher than those of the circular bearing system; the *AMF* values of the laminated rubber bearing system are higher than those of the PTFE–rubber bearing

system; and the *AMF* values of the CR bearing system are higher than those of the NR bearing system. However, the order of the variation amplitude from largest to smallest is as follows: Chi-Chi excitation, Imperial Valley excitation and Kobe excitation, which again verifies the high sensitivity of the system to long-duration excitations.

5. Conclusions

Based on shaking table tests on the double-column pier-bearing system, three typical ground motions (Imperial Valley excitation, Kobe excitation, and Chi-Chi excitation) were adapted to analyze the effects of bearing thickness, shape, type, and material on the seismic behaviors of the system. The main conclusions are as follows:

1. As the bearing thickness increases, the peak displacement of the system decreases from 11.41 mm to 10.28 mm, with a reduction amplitude of 10%; the damping ratio decreases from 9.7% to 4.1%, a reduction of 58%. However, a larger damping ratio is desired from the perspective of seismic energy dissipation. Therefore, there is a trade-off between bearing thickness and the system's displacement as well as damping ratio, and careful verification should be conducted during selection.
2. The peak displacement of the system with circular bearings is 7% lower than that with square bearings, while the damping ratio of the circular bearing system is 58% higher than that of the square bearing system, indicating that circular bearings exhibit superior seismic performance.
3. The seismic isolation performance of NR bearings is slightly better than that of CR bearings. NR bearings are suitable for scenarios where it is necessary to extend the structural period to avoid resonance, while CR bearings are preferred for scenarios requiring increased stiffness to reduce displacement.
4. PTFE–rubber bearings are suitable for long-period earthquakes, whereas ordinary laminated rubber bearings are more applicable to short-period pulse-type earthquakes.
5. The cumulative effect of long-duration earthquakes is significant. Even with a lower PGA, the displacement response may be greater than that of short-duration earthquakes with a higher PGA.
6. Wavelet transform can accurately identify the natural vibration frequency (0.5~1.2 Hz) and damping ratio (3~9%) of the system, but it has limitations in separating the responses of pulse-type signals.
7. The above results are derived from scaled model tests, and it is necessary to collect actual field signals when investigating practical pier systems.

Author Contributions: Conceptualization, H.Z.; methodology, H.Z.; formal analysis, H.Z. and J.L.; investigation, J.L. and Y.L.; writing—original draft preparation, H.Z. and J.L.; writing—review and editing, Y.L. All authors have read and agreed to the published version of the manuscript.

Funding: This work was supported by the National Natural Science Foundation of China (Grant No. 52208201).

Data Availability Statement: The data presented in this study are available on request from the corresponding author.

Conflicts of Interest: The authors declare no conflicts of interest.

References

1. Gao, H.; Xia, W.; Liu, G. Analysis of Seismic Performance for Segmentally Assembled Double-Column Bridge Structures Based on Equivalent Stiffness. *Buildings* **2025**, *15*, 1919. [CrossRef]
2. Dong, H.; Feng, W.; Zheng, Z.; Han, Q.; Du, X. Experimental Investigation on Failure Mechanism and Hysteresis Behavior of RC Single- and Double-Column Piers. *J. Bridge Eng.* **2024**, *29*, 04024094. [CrossRef]

3. Gu, C.; Wang, X.; Zhou, X.; Li, X.; Liao, Y.; Zheng, N. Seismic Behavior of Prefabricated Thin-Walled CFST Double-Column Bridge Piers. *Thin-Walled Struct.* **2024**, *198*, 111654. [CrossRef]
4. Crespi, P.; Zucca, M.; Valente, M. On the collapse evaluation of existing RC bridges exposed to corrosion underhorizontal loads. *Eng. Fail. Anal.* **2020**, *116*, 104727. [CrossRef]
5. Liu, J.; Li, M.; Zhang, G. Seismic Performance of UHPC Precast Double-Column Piers with Socket Connections. *Mater. Struct.* **2025**, *58*, 122. [CrossRef]
6. Hu, S.; Hu, R.; Yang, M.; Meng, D. Influence of the Deteriorated Anti-Seismic Devices on Seismic Performance and Device Behavior of Continuous Girder Bridges. *Earthq. Struct.* **2023**, *24*, 333–343. [CrossRef]
7. Muscarella, J.V. An Experimental Study of Elastometric Bridge Bearings with Design Recommendations. Ph.D. Thesis, The University of Texas at Austin, Austin, TX, USA, 1995.
8. Nettis, A.; Mucci, V.M.; Ruggieri, S.; Uva, G. Seismic fragility and risk assessment of isolated bridges subjected to pre-existing ground displacements. *Soil. Dyn. Earthq. Eng.* **2025**, *194*, 109335. [CrossRef]
9. Zhang, Z.; Vassiliou, M.F.; Zhou, Y.; Reyes, S.I.; Konstantinidis, D. Experimental and Numerical Studies on Thick Rubber Bearings under Uniaxial and Offset Tensile Loading. *J. Struct. Eng.* **2024**, *150*, 04024070. [CrossRef]
10. Mori, A. Investigation of the Behaviour of Seismic Isolation Systems for Bridges. Ph.D. Thesis, University of Canterbury, Christchurch, New Zealand, 1993.
11. Han, Y.; Dong, J.; Wang, L. Experimental Study on the Seismic Performance of Socket Bridge Piers. *Adv. Civ. Eng.* **2020**, *2020*, 8895196. [CrossRef]
12. Xiang, N.; Li, J. Experimental and Numerical Study on Seismic Sliding Mechanism of Laminated-Rubber Bearings. *Eng. Struct.* **2017**, *141*, 159–174. [CrossRef]
13. Xiang, N.; Huang, J.; Wang, J.; Xu, H.; Wu, S. An Innovative Sliding-Controllable Laminated Rubber Bearing for Enhancing Seismic Performance of Highway Bridges. *Eng. Struct.* **2024**, *319*, 118877. [CrossRef]
14. Xu, Y.; Zeng, Z.; Wang, Z.; Ge, J. Experimental Studies of Embedment Length of Precast Bridge Pier with Socket Connection to Pile Cap. *Eng. Struct.* **2021**, *233*, 111906. [CrossRef]
15. Koo, G.-H.; Lee, J.-H.; Lee, H.-Y.; Yoo, B. Stability of Laminated Rubber Bearing and Its Application to Seismic Isolation. *KSME Int. J.* **1999**, *13*, 595–604. [CrossRef]
16. Ramli, M.Z.; Adnan, A.; Tan, C.W. Performance of Isomeric and Spiral Plate Rubber Bearing Base Isolator System in Bridges. In Proceedings of the International Conference on Earthquake Engineering and Seismology (IZIIS-50), Skopje, Macedonia, 18–21 May 2015.
17. Peng, L.; Li, Z.; Luo, W.; Li, Y. Analysis of Dynamic Viscoelastic Properties of Chloroprene Rubber Considering Pre-Strain Effect. *Mater. Res. Express* **2019**, *6*, 105324. [CrossRef]
18. Lotfi, V.; Roesset, J.M.; Tassoulas, J.L. A Technique for the Analysis of the Response of Dams to Earthquakes. *Earthq. Eng. Struct. Dyn.* **1987**, *15*, 463–489. [CrossRef]
19. Lee, J.H.; Cho, J.-R. Simplified Earthquake Response Analysis of Rectangular Liquid Storage Tanks Considering Fluid-Structure Interactions. *Eng. Struct.* **2024**, *300*, 117157. [CrossRef]
20. Sheena, A.D. Seismic Noise Removal and Its Applications—A Review of Exploring Wavelet Transform in Civil Engineering. *Int. J. Civ. Eng.* **2017**, *4*, 1–6. [CrossRef]
21. Basu, B.; Gupta, V.K. Wavelet-Based Non-Stationary Response Analysis of a Friction Base-Isolated Structure. *Earthq. Eng. Struct. Dyn.* **2000**, *29*, 1659–1676. [CrossRef]
22. Yanni, H.; Fragiadakis, M.; Mitseas, I.P. Wavelet-Based Stochastic Model for the Generation of Fully Nonstationary Bidirectional Seismic Accelerograms. *Earthq. Eng. Struct. Dyn.* **2025**, *54*, 1397–1416. [CrossRef]
23. Sun, Z.; Chang, C. Structural Damage Assessment Based on Wavelet Packet Transform. *J. Struct. Eng.* **2002**, *128*, 1354–1361. [CrossRef]
24. *GB 50010-2010*; Code for Design of Concrete Structures. Ministry of Housing and Urban—Rural Development of the People's Republic of China: Beijing, China.
25. Hartzell, S.; Helmberger, D.V. Strong-Motion Modeling of the Imperial Valley Earthquake of 1979. *Bull. Seismol. Soc. Am.* **1982**, *72*, 571–596.
26. Qu, S.-S.; Chen, Y.; Lv, Y. Centrifuge Shaking Table Tests on a Friction Pendulum Bearing Isolated Structure with a Pile Foundation in Soft Soil. *Earthq. Struct.* **2022**, *23*, 517–526. [CrossRef]
27. Tamura, K. Seismic Design of Highway Bridge Foundations with the Effects of Liquefaction since the 1995 Kobe Earthquake. *Soils Found.* **2014**, *54*, 874–882. [CrossRef]
28. Zhou, S.-H.; Feng, Z.-J.; Zhang, C.; Zhang, C.-C.; Wang, J.-K.; Wang, S.-Q. Dynamic Response and Damage Analysis of Variable Section Pile Group Foundation at Liquefaction Site Under Different Seismic Intensities. *Buildings* **2025**, *15*, 3840. [CrossRef]
29. Kim, S.H.; Mha, H.S.; Lee, S.W. Effects of bearing damage upon seismic behaviors of a multi-span girder bridge. *Eng. Struct.* **2006**, *28*, 1071–1080. [CrossRef]

30. Heykoop, I.; Woods, J.E.; Hoult, N.A.; Coveney, M. Case Study of Long-Term Bearing and Expansion Joint Movement on a Prestressed Concrete Bridge. *J. Bridge Eng.* **2025**, *30*, 7073. [CrossRef]
31. Maleki, S. Deck Modeling for Seismic Analysis of Skewed Slab-Girder Bridges. *Eng. Struct.* **2002**, *24*, 1315–1326. [CrossRef]
32. Tang, H.; Li, J. Displacement Control Method for Continuous Bridges on Laminated Rubber Bearings Under Earthquake Excitation. *China J. Highw. Transp.* **2013**, *26*, 110–116. [CrossRef]
33. Liu, Z. Reconnaissance and Preliminary Observations of Bridge Damage in the Great Wenchuan Earthquake, China. *Struct. Eng. Int.* **2009**, *19*, 277–282. [CrossRef]
34. Kang, X.; Jiang, L.; Bai, Y.; Caprani, C.C. Seismic Damage Evaluation of High-Speed Railway Bridge Components under Different Intensities of Earthquake Excitations. *Eng. Struct.* **2017**, *152*, 116–128. [CrossRef]
35. Agrahari, R.K.; Pathak, K.K. Floor Acceleration Amplification Factor in Yielding of Moment Resisting RC Frame Structures. *Indian J. Eng. Mater. Sci. IJEMS* **2023**, *30*, 138–146. [CrossRef]
36. Latif, I.; Surana, M.; Banerjee, A. Investigating In-Structure Acceleration Amplification Factor of RC Frames Using Explainable Artificial Intelligence. *Structures* **2025**, *79*, 109592. [CrossRef]
37. Shi, Y.; Lei, L.; Yan, M.; Gu, X. Amplification Effect and Influencing Factors of Rebound-Collision Impact Amplifier. *J. Vib. Control* **2025**, *31*, 2550–2559. [CrossRef]
38. Bassett, K.; Carriveau, R.; Ting, D.S.-K. Vibration Analysis of 2.3 MW Wind Turbine Operation Using the Discrete Wavelet Transform. *Wind Eng.* **2010**, *34*, 375–388. [CrossRef]
39. He, W.; Guo, Z.; Li, C.; Wang, W.; Wei, B.; Shao, P.; Zeng, Y. Data-Driven Simulation of Near-Fault Ground Motions Using Stationary Wavelet Transform and Hilbert Analysis. *Buildings* **2025**, *15*, 4219. [CrossRef]
40. Ülker-Kaustell, M.; Karoumi, R. Application of the Continuous Wavelet Transform on the Free Vibrations of a Steel–Concrete Composite Railway Bridge. *Eng. Struct.* **2011**, *33*, 911–919. [CrossRef]
41. Vamsi, I.; Hemanth, M.P.; Kumar Penumakala, P.; Sabareesh, G.R. Damage Monitoring of Pultruded GFRP Composites Using Wavelet Transform of Vibration Signals. *Measurement* **2022**, *195*, 111177. [CrossRef]
42. Ito, M.; Okada, S.; Kuriyama, I. The deterioration of mechanical properties of chloroprene rubber in various conditions. *J. Mater. Sci.* **1981**, *16*, 10–16. [CrossRef]

Disclaimer/Publisher's Note: The statements, opinions and data contained in all publications are solely those of the individual author(s) and contributor(s) and not of MDPI and/or the editor(s). MDPI and/or the editor(s) disclaim responsibility for any injury to people or property resulting from any ideas, methods, instructions or products referred to in the content.